Hindawi Publishing Corporation
Journal of Atomic, Molecular, and Optical Physics
Volume 2011, Article ID 452026, 9 pages
doi:10.1155/2011/452026

Research Article

Photoionization Processes of the Single-Ionized Boron

Ju-Tang Hsiao,[1] Hsiao-Ling Sun,[2] Sheng-Fang Lin,[2] and Keh-Ning Huang[2,3]

[1] *Department of Natural Sciences, National Institute for Compilation and Translation, Taipei 10644, Taiwan*
[2] *Institute of Atomic and Molecular Sciences, Academia Sinica, P.O. Box 23-166, Taipei 10617, Taiwan*
[3] *Department of Physics, National Taiwan University, Taipei 10617, Taiwan*

Correspondence should be addressed to Ju-Tang Hsiao, jthsiao@ntu.edu.tw

Received 1 October 2010; Accepted 16 January 2011

Academic Editor: Miron Ya Amusia

The relativistic calculations of the cross-section σ, the angular-distribution parameter β, and spin-polarization parameters $\{\xi, \eta, \zeta\}$ of photoelectrons using the multiconfiguration relativistic random-phase approximation theory for the photoionization of the B^+ ion are presented. Precise energies and widths of all five Rydberg series of doublyexcited states $(2pns)^1P_1^o$, $(2pns)^3P_1^o$, $(2pnd)^1P_1^o$, $(2pnd)^3P_1^o$, and $(2pnd)^3D_1^o$ are determined. Our predictions are in very close agreement with experiments and are consistent with other calculations.

1. Introduction

Experimental and theoretical studies of photoionization processes are of fundamental importance because they have greatly increased the understanding of the responses of atoms or ions to electromagnetic radiations. In recent years, the development of merged ion-photon beams and third-generation synchrotron radiation facilities provides sufficiently high density of target ions and the required incident photon flux. These high-resolution measurements attributed to rapidly evolving experimental techniques enhanced the ability to study the photoionization of atomic systems along isoelectronic, isonuclear, and isoionic series.

Divalence atomic systems such as the Be-isoelectronic sequence are attractive candidates for the systematic studies of the photoionization processes because of their relatively simple quasi-two-electron structure. In these atomic systems, two loosely bound electrons in the L-shell are well separated from the other two tightly bound K-shell electrons. They are suitable for comprehensive studies of electron-correlation and relativistic effects in photoionization processes. In addition, many works have shown that relativistic effects play an important role in the photoionization of small atoms, such as Be [1–4], Ne [5], and Mg [6–8]. Therefore, it is worthwhile to investigate the interplay between electron-correlation and relativistic effects on the photoionization of atoms or ions with a low nuclear charge.

Considerable theoretical and experimental efforts have been made recently to investigate the photoionization of the B^+ ion. Among the theoretical results are the R-matrix calculations of Tully et al. [9, 10], the B-spline-based configuration-interaction approach of Chang and Zhu [11], and the noniterative eigenchannel R-matrix method of Kim and Manson [12].

On the experimental side, the absorption spectrum of B^+ has been measured by Esteva [13]. Jannitti et al. [14] investigated the absorption spectrum of B^+ for photon energies between 400 and 1700 Å by using two-laser produced plasma. Recently, a good agreement between theory and experiment for the photoionization of the B^+ ion was performed by Schippers et al. [15] by using a photon-ion merged-beams arrangement at the advanced light source. They also calculated the photoionization cross section using the semirelativistic Breit-Pauli R-matrix approach.

The multiconfiguration relativistic random-phase approximation theory (MCRRPA) has been successfully applied to photoexcitation [16–29] and photoionization [1, 8, 28, 30–34] of divalence atomic systems. Double-excitation resonances in the photoionization spectrum reveal electron-correlation and relativistic effects and therefore provide a stringent testing ground for the accuracy of theoretical models. In the photon-energy region between $(1s^22s)^2S_{1/2}$ and $(1s^22p)^2P_{1/2}^o$ ionization thresholds of the B^+ ion, double-excitation autoionization resonances are the most

prominent feature in its photoionization spectrum. These double-excitation resonances may be classified into five Rydberg series: $(2pns)^1P_1^o$, $(2pns)^3P_1^o$, $(2pnd)^1P_1^o$, $(2pnd)^3P_1^o$, and $(2pnd)^3D_1^o$.

Most of the earlier nonrelativistic studies have focused only on two singlet Rydberg series $(2pns)^1P_1^o$ and $(2pnd)^1P_1^o$. In the nonrelativistic calculation, the cross section should be similar to the MCRRPA result but without the extremely sharp resonance structures of triplet resonances $(2pns)^3P_1^o$, $(2pnd)^3P_1^o$, and $(2pnd)^3D_1^o$. These resonances are the result of relativistic effects, without which they are completely forbidden. Because of the incorporation of relativity in the MCRRPA calculation, the double-excitation resonances in the photoionization spectrum belonging to all five Rydberg series of the B^+ ion are built-in from the outset.

The main concerns of most photoionization researches are with the corss section. Nevertheless, a complete macroscopic analysis of photoionization processes also requires knowledge of the angular distribution and spin polarization of photoelectrons. In the nonrelativistic limit, these extra parameters are all constant. In this work, we continue our previous investigation of the photoionization processes of the B^+ ion by using the MCRRPA theory [35]. The cross section, angular distribution, and spin polarization of photoelectrons including all five Rydberg series of low-lying doubly excited states $(2pns)^1P_1^o$, $(2pns)^3P_1^o$, $(2pnd)^1P_1^o$, $(2pnd)^3P_1^o$, and $(2pnd)^3D_1^o$ are studied in detail, accounting for all relativistic excitation channels. In Section 2, we review our method briefly. Results are presented in Section 3, and the conclusion is made in Section 4.

2. MCRRPA Theory

A detailed formulation of the MCRRPA has been given in previous papers [36, 37], and only a summary of the essential features will be given here. The N-electron atomic system is described as a superposition of configuration wavefunctions with time-dependent weights. The time-dependent variational principle is employed to determine the response of the atomic system to a time-dependent external field. The resulting terms independent of the external field lead to the usual multiconfiguration Dirac-Fock (MCDF) description of an atomic state. Those terms proportional to the external field lead to the MCRRPA equations describing the linear response of the atomic state to the external field. If we start from a single-configuration reference state, the MCRRPA equations reduce to the relativistic random-phase approximation (RRPA) equations. The multiconfiguration reference state is described by a linear combination of three configurations with two valence electrons coupled to zero angular momentum and even parity:

$$\Psi = C_1\left(1s_{1/2}^2 2s_{1/2}^2\right)_0 + C_2\left(1s_{1/2}^2 2p_{1/2}^2\right)_0 + C_3\left(1s_{1/2}^2 2p_{3/2}^2\right)_0, \quad (1)$$

where C_1, C_2, and C_3 are configuration-weight coefficients.

We consider seven excitation channels from the valence electrons in the electric-dipole approximation for photon energies between $(1s^2 2s)^2S_{1/2}$ and $(1s^2 2p)^2P_{1/2}^o$ ionization thresholds.

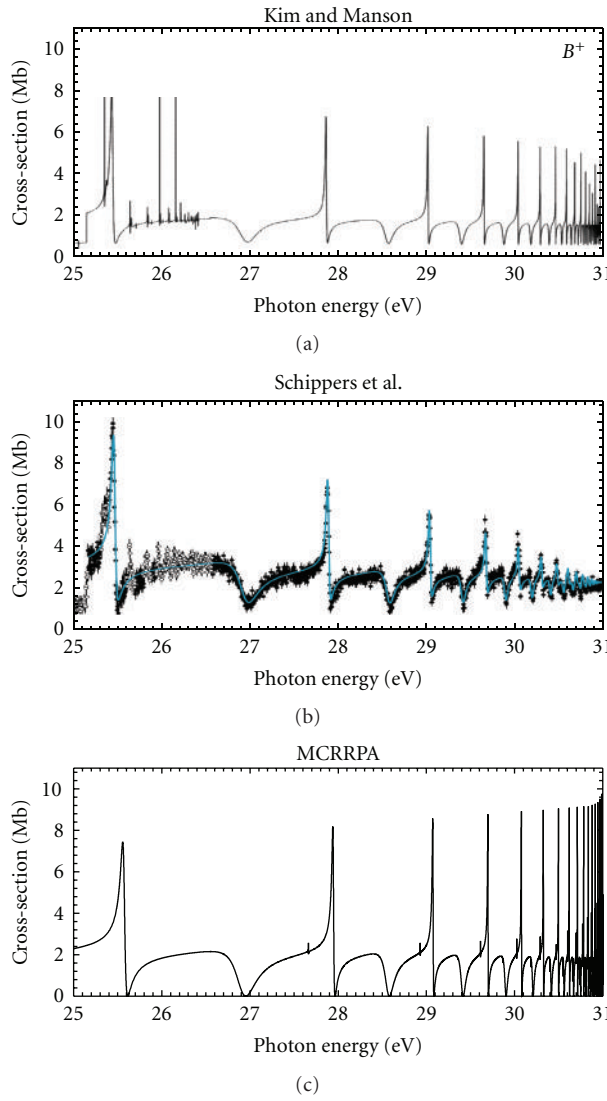

Figure 1: Comparison of the photoionization cross section of the B^+ ion from the present MCRRPA calculation with those from others.

(i) Photoionization channels:

(a) $(2s^2)^1S_0 \rightarrow (2s\epsilon p)^1P_1^o$,
(b) $(2s^2)^1S_0 \rightarrow (2s\epsilon p)^3P_1^o$.

(ii) Photoexcitation channels:

(c) $(2p^2)^1S_0 \rightarrow (2pns)^1P_1^o$, $n \geq 3$,
(d) $(2p^2)^1S_0 \rightarrow (2pns)^3P_1^o$,
(e) $(2p^2)^1S_0 \rightarrow (2pnd)^1P_1^o$,
(f) $(2p^2)^1S_0 \rightarrow (2pnd)^3P_1^o$,
(g) $(2p^2)^1S_0 \rightarrow (2pnd)^3D_1^o$.

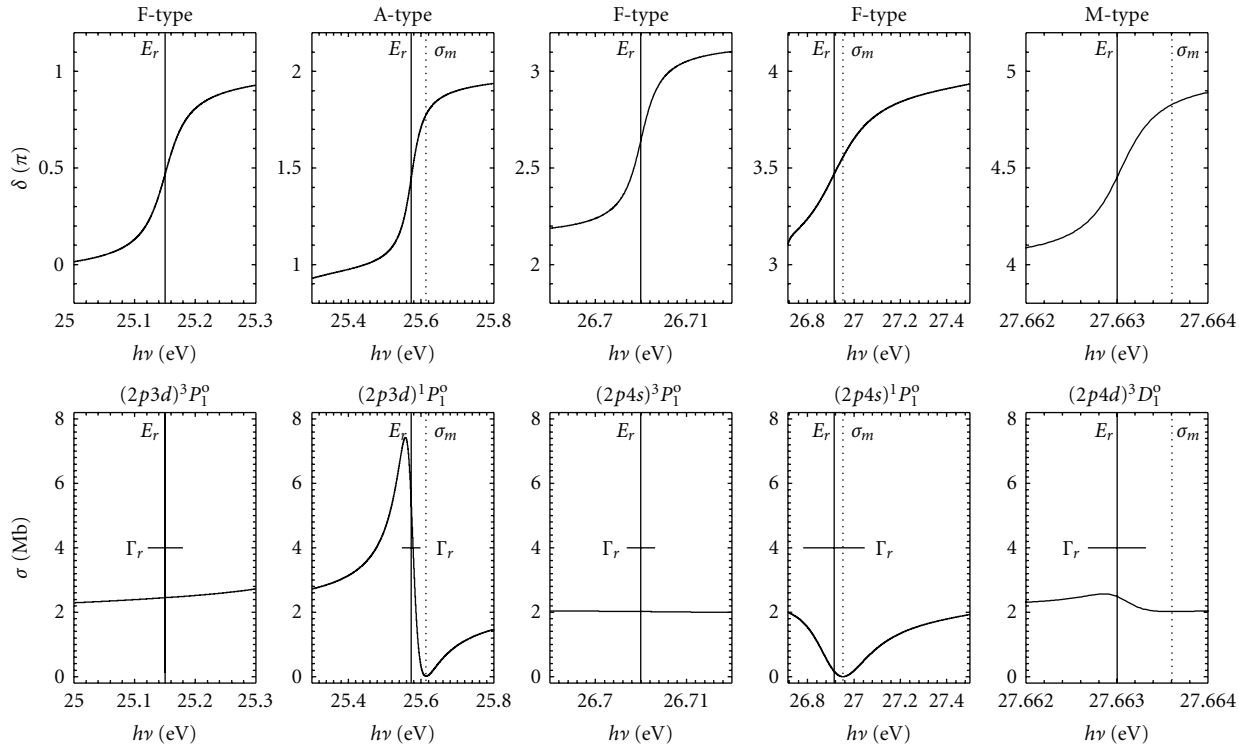

FIGURE 2: Photoionization cross sections σ and corresponding phase shifts δ of the first five resonances. Here, σ_m indicates the cross-section minimum, E_r the resonance energy, and Γ_r the width of the resonance.

The couplings between the *photoionization* and *photoexcitation channels* generate five autoionization resonance series in the photoionization spectrum.

Photoionization of unpolarized atoms or ions in the dipole approximation can be completely described by a set of five dynamical parameters [38–40], namely, the total cross section σ, the angular-distribution parameter β, and spin-polarization parameters ξ, η, and ζ. At the photon energy $\hbar\omega$, these dynamical parameters for the photoionization of the B^+ ion can be expressed in terms of photoionization amplitudes D_S, D_T, and the relative phase $\phi \equiv \phi_S - \phi_T$, where the subscripts S and T denote, respectively, the singlet and triplet channels:

$$\sigma = \frac{8\pi^4}{\omega c}\left(|D_S|^2 + |D_T|^2\right), \tag{2}$$

$$\beta = \frac{2|D_S|^2 - |D_T|^2}{|D_S|^2 + |D_T|^2}, \tag{3}$$

$$\xi = \frac{3}{\sqrt{2}}\frac{|D_S||D_T|}{|D_S|^2 + |D_T|^2}\cos\phi, \tag{4}$$

$$\eta = \frac{3}{\sqrt{2}}\frac{|D_S||D_T|}{|D_S|^2 + |D_T|^2}\sin\phi, \tag{5}$$

$$\zeta = \frac{3}{2}\frac{|D_T|^2}{|D_S|^2 + |D_T|^2} = 1 - \frac{1}{2}\beta. \tag{6}$$

We note particularly that for photoionization of an unpolarized B^+ ion, only three of the five parameters $\{\sigma, \beta, \xi, \eta, \zeta\}$ are independent, which may be expressed in terms of three independent quantities $\{|D_S|, |D_T|, \phi\}$.

3. Results and Discussions

In the present work, we investigate the photoionization spectrum of the B^+ ion in the region of interest by using the MCRRPA theory. We consider the incident photon with energy between the ionization thresholds $(1s^22s)^2S_{1/2}$ and $(1s^22p)^2P^o_{1/2}$, where only photoionization channels (a) and (b) are open. The couplings of the two photoionization channels and remaining five photoexcitation channels provide the paths for the doubly excited states to decay through autoionization. As a result, the photoionization cross section in the range is dominated by the five Rydberg series of resonances $(2pns)^1P_1^o$, $(2pns)^3P_1^o$, $(2pnd)^1P_1^o$, $(2pnd)^3P_1^o$, and $(2pnd)^3D_1^o$. The comparison of our photoionization cross section with those of selected theory and expreiment is presented in Figure 1. In our calculation, predicted profiles of the autoionization resonances are in very close agreement with experimental measurements.

The curve in Figure 1(c) represents the seven-channel MCRRPA calculation which shows all five Rydberg series of resonances obtained from the couplings of the two photoionization channels with all five photoexcitation channels. The photoionization cross section is characterized by a nonresonant background of about 2 Mb with resonance structures. Because the photoionization continuum $(2s\epsilon p)^1P_1^o$ and

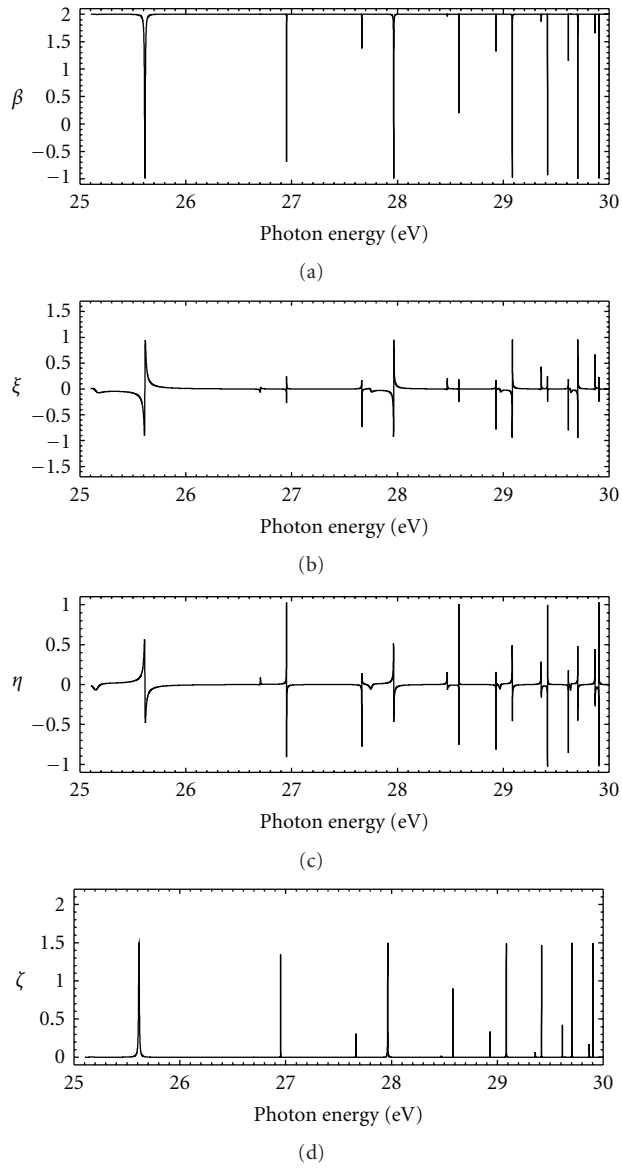

FIGURE 3: The angular-distribution and spin-polarization parameters $\{\beta, \xi, \eta, \zeta\}$ for photoelectrons by seven-channel MCRRPA calculations in the double-excitation resonance region.

the double-excitation series $(2pns)^1P_1^o$ and $(2pnd)^1P_1^o$ all arise from the $n = 2$ atomic complex and with the same total spin and orbital angular-momenta, the couplings between them are strong so that the characteristics of the cross section are completely dominated by double-excitation resonances $(2pns)^1P_1^o$ and $(2pnd)^1P_1^o$. The Rydberg series $(2pns)^1P_1^o$ appear as broad autoionizing resonances in the photoionization cross-section while the narrower Rydberg series $(2pnd)^1P_1^o$ is sandwiched amid the Rydberg series $(2pns)^1P_1^o$. The strong couplings between doubly excited states $(2pns)^1P_1^o$ and the continuum $(2s\epsilon p)^1P_1^o$ give rise to broad resonances; however, the narrower resonances are due to the weaker couplings between states $(2pnd)^1P_1^o$ and continuum $(2s\epsilon p)^1P_1^o$. Broad resonances indicate short lifetimes of the corresponding doubly excited states while the narrow profiles reveal long lifetimes.

Photoionization cross sections σ and corresponding phase shifts δ of the first five resonances are shown in Figure 2 as a demonstration, where σ_m indicates the cross-section minimum, E_r the resonance energy, and Γ_r the width of the resonance. The phase shift δ increases π in the vicinity of each resonance; a slower variation in the phase shift indicates a broader resonance, that is, a shorter lifetime. Phase-shift variations allow us to identify theoretically precise positions and widths of pseudobound states. The precise positions E_r and widths Γ_r of double-excitation resonances belonging to five Rydberg series for the MCRRPA calculation are derived from phase-shift variations.

The allowed double-excited states $(2pns)^1P_1^o$ and $(2pnd)^1P_1^o$ are well separated for a parametric fit to be made in the way suggested by Dubau and Seaton [41], within the framework of the quantum defect theory. In Tables 1 and 2, we present effective quantum numbers ν, quantum defects μ, resonance energies E_r, and the Beutler-Fano parameter q [42], which describe the resonance profiles. Table 3 present the resonance widths Γ_r of allowed doubly excited states $(2pns)^1P_1^o$ and $(2pnd)^1P_1^o$ of our MCRRPA calculations and other currently available data. Our present calculations are compared with theoretical results of Tully et al. [9, 10], Chang and Zhu [11], and Kim and Manson [12]. Experimental results of Esteva [13], Jannitti et al. [14], and Schippers et al. [15] are also listed for comparison. The quantum defects μ of the $(2pns)^1P_1^o$ series are positive and those of the $(2pnd)^1P_1^o$ series are negative and small. It shows a fair agreement of our predicted positions E_r and widths Γ_r, as well as parameters ν, μ, and q of the series $(2pns)^1P_1^o$ and $(2pnd)^1P_1^o$ with those of previous results. In Tables 4, 5, and 6, we present the effective quantum numbers ν, quantum defects μ, resonance energies E_r, and resonance widths Γ_r of doubly excited states $(2pns)^3P_1^o$, $(2pnd)^3P_1^o$, and $(2pnd)^3D_1^o$ of B^+ from the MCRRPA calculation.

Physically, the coupling strength between the bound and continuum components of the wave function of a doubly excited state is measured by the resonant width Γ_r, which also determines the nonradiative decay rate of an autoionization state. Because the orbital symmetries of the photoionization channels $(2s\epsilon p)^3P_1^o$ and $(2s\epsilon p)^1P_1^o$ are of P-type, the coupling of resonances $(2pnd)^3D_1^o$ with these photoionization channels are weaker such that their widths are much narrower. There are, however, some discrepancies between theoretical results for resonance widths. Our MCRRPA calculation, which deals with all five Rydberg series, includes relativistic and correlation in an *ab initio* manner and treats the initial and final states in a balanced fashion; therefore, it should in principle provide reliable lifetimes within the model itself.

In comparison with our previous MCRRPA results for neutral Be [3], the stronger nuclear field of the B^+ ion moves a number of the near-threshold resonances below the ionization threshold of the B^+ ion and thereby alters the behavior of the cross section considerably. In addition, the couplings among the resonances are greater for the B^+ ion than

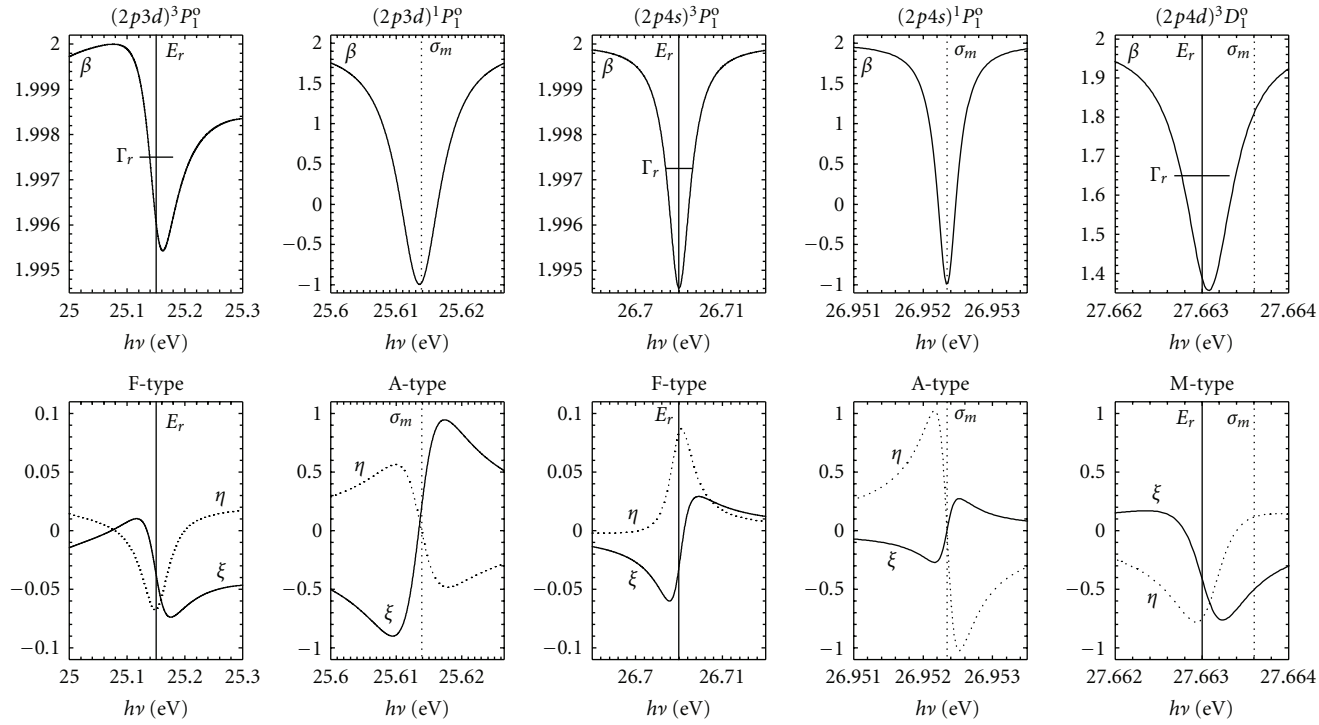

FIGURE 4: The angular-distribution and spin-polarization parameters $\{\beta, \xi, \eta\}$ for A-type resonances $(2p3d)^1P_1^o$ and $(2p4s)^1P_1^o$, F-type resonances for $(2p3d)^3P_1^o$ and $(2p4s)^3P_1^o$, and M-type resonances for $(2p4d)^3D_1^o$. Here, σ_m indicates the cross-section minimum, E_r the resonance energy, and Γ_r the width of the resonance.

the Be atom, because the energy gap between $(1s^22s)^2S_{1/2}$ and $(1s^22p)^2P_{1/2}^o$ thresholds of the B^+ ion are smaller than that of the Be atom. This compression leads to the implication that couplings of resonances will become stronger for the photoionization of higher members of the Be isoelectronic sequence.

The angular-distribution and spin-polarization parameters $\{\beta, \xi, \eta, \zeta\}$ for photoelectrons by seven-channel MCR-RPA calculations in the double-excitation resonance region are given in Figure 3. These parameters deviate from their nonrelativistic limits due to relativistic effects which permit couplings with forbidden channels. In the nonrelativistic limit, the final state should be of the $^1P_1^o$ type and $D_T = 0$ such that $\beta = 2$ and $\xi = \eta = \zeta = 0$. All these parameters, which have varied sharply at locations of resonances, display primarily three classes of characteristic behaviors, A-type for *allowed* resonances $(2pns)^1P_1^o$ and $(2pnd)^1P_1^o$, F-type for *forbidden* resonances $(2pns)^3P_1^o$ and $(2pnd)^3P_1^o$, and M-type for *forbidden* resonances $(2pnd)^3D_1^o$, which resemble a *mixture* of A-type and F-type.

The parameters $\{\beta, \xi, \eta\}$ for A-type resonances $(2p3d)^1P_1^o$ and $(2p4s)^1P_1^o$, F-type resonances for $(2p3d)^3P_1^o$ and $(2p4s)^3P_1^o$, and M-type resonance for $(2p4d)^3D_1^o$ around the resonances are given in Figure 4 as a demonstration. Around the A-type resonances, we observe marked departures of β from its background value 2, and β reaches its minimum -1 at the resonance minimum σ_m. The parameters ξ and η change sign through the resonance minimum and vary reciprocally to the energy departure from the resonance minimum. Furthermore, it is worth noting that although the cross section in (2) is independent of the relative phase, the resonance minimum reveal the position where the relative phase goes through π rapidly. In the neighborhood of F-type resonances, the variations of photoionization parameters are much smaller and less symmetric about the resonance energy E_r, compared to those of the A-type resonances. It is also reasonable that the variations of β and ζ reach their extrema near the resonance energy E_r for resonances $(2p3d)^3P_1^o$ and $(2p4s)^3P_1^o$, and the half-width of the variations is also approximately the resonance width Γ_r. The resonance structures of photoionization parameters for the M-type resonance $(2p4d)^3D_1^o$ take place at the resonance energy E_r, which resembles that of F-type whereas a very deep cross section minimum also occurs near the $(2p4d)^3D_1^o$ resonance structure, similar to that of A-type. These near-resonance characteristics of the interesting *detuning* for photoionization parameters of photoelectrons from the Single-Ionized boron share the similar features of those from the neutral beryllium [3] and may be understood by considering the behaviors of photoionization amplitudes D_S, D_T, and the relative phase ϕ.

4. Conclusion

In summary, notable features in the processes of the simultaneous excitation of two valence electrons of the B^+ ion by a single photon are the double-excitation resonances in the photoionization spectrum, angular distributions, and spin

Table 1: Comparison of effective quantum numbers ν, quantum defects μ, resonance energies E_r (in eV), and profile parameters q of doubly excited states $(2pns)^1P_1^o$ of B^+ from theories and experiments.

	ν			μ	E_r (eV)					q	
State	Present	[11]	[12]	Present	Present	[14]	[9]	[12]	[15]	Present	[15]
$(2p4s)^1P_1^o$	3.58398749	3.6014	3.6036	0.41590601	26.9137	26.91	26.96	26.9405	26.923	−0.30281	−0.46(3)
$(2p5s)^1P_1^o$	4.58645218	4.6003	4.5994	0.41344131	28.5634	28.58	28.59	28.5568	28.580	−0.29740	−0.22(3)
$(2p6s)^1P_1^o$	5.58917807	5.5995	5.5975	0.41071543	29.4084	29.44	29.42	29.3924	29.420	−0.29246	−0.16(5)
$(2p7s)^1P_1^o$	6.59248356	6.5994	6.5966	0.40740993	29.8983			29.8787	29.895	−0.29025	−0.34(7)
$(2p8s)^1P_1^o$	7.59693592	7.5994	7.5955	0.40295757	30.2075			30.1861	30.205	−0.28880	−0.35(9)
$(2p9s)^1P_1^o$	8.60267519		8.5952	0.39721830	30.4151			30.3927	30.409	−0.29036	−0.4(2)
$(2p10s)^1P_1^o$	9.61018655		9.5944	0.38970694	30.5612			30.5382	30.562	−0.29370	−0.2(3)
$(2p11s)^1P_1^o$	10.61981847		10.5953	0.38007502	30.6680			30.6444		−0.29820	
$(2p12s)^1P_1^o$	11.63196241		11.5927	0.36793108	30.7483			30.7244		−0.30278	
$(2p13s)^1P_1^o$	12.64717198			0.35272151	30.8103					−0.30577	
$(2p14s)^1P_1^o$	13.66560285			0.33429064	30.8591					−0.30698	
$(2p15s)^1P_1^o$	14.68741014			0.31248335	30.8982					−0.30498	
$(2p16s)^1P_1^o$	15.71318796			0.28670553	30.9301					−0.30013	
$(2p17s)^1P_1^o$	16.74273514			0.25715835	30.9564					−0.29126	
$(2p18s)^1P_1^o$	17.77644603			0.22344747	30.9783					−0.27782	
$(2p19s)^1P_1^o$	18.81451302			0.18538047	30.9968					−0.25592	
$(2p20s)^1P_1^o$	19.85735657			0.14253693	31.0125					−0.21239	

Table 2: Comparison of effective quantum numbers ν, quantum defects μ, resonance energies E_r (in eV), and profile parameters q of doubly excited states $(2pnd)^1P_1^o$ of B^+ from theories and experiments.

	ν			μ	E_r (eV)						q	
State	Present	[11]	[12]	Present	Present	[14]	[9]	[12]	[13]	[15]	Present	[15]
$(2p3d)^1P_1^o$	3.12372213	3.0948	3.0891	−0.12375763	25.5731	25.43	25.47	25.4262	25.44	25.458(1)	−1.58033	−2.21(8)
$(2p4d)^1P_1^o$	4.12062029	4.0883	4.0862	−0.12065579	27.9453	27.91	27.90	27.8610	27.90	27.889(1)	−1.74855	−1.86(6)
$(2p5d)^1P_1^o$	5.12036077	5.0849	5.0753	−0.12039627	29.0747	29.06	29.05	29.0166	29.04	29.041(1)	−1.83648	−2.0(1)
$(2p6d)^1P_1^o$	6.12180122	6.0832	6.0720	−0.12183672	29.6983	29.70	29.68	29.6533		29.676(1)	−1.88850	−2.3(2)
$(2p7d)^1P_1^o$	7.12467028	7.0824	7.0708	−0.12470578	30.0784			30.0408		30.064(2)	−1.92160	−1.9(2)
$(2p8d)^1P_1^o$	8.12901572		8.0689	−0.12905122	30.3269			30.2935		30.320(2)	−1.94378	−1.4(3)
$(2p9d)^1P_1^o$	9.13497539		9.0681	−0.13501089	30.4983			30.4676		30.490(4)	−1.96123	−1.8(7)
$(2p10d)^1P_1^o$	10.14277810		10.0668	−0.14281360	30.6215			30.5924		30.61(1)	−1.97372	−2(3)
$(2p11d)^1P_1^o$	11.15267006		11.0667	−0.15270556	30.7130			30.6850			−1.98510	
$(2p12d)^1P_1^o$	12.16500247		12.0664	−0.16503797	30.7828			30.7556			−2.00091	
$(2p13d)^1P_1^o$	13.18004710			−0.18008260	30.8372						−2.00782	
$(2p14d)^1P_1^o$	14.19816003			−0.19819553	30.8805						−2.02644	
$(2p15d)^1P_1^o$	15.21966360			−0.21969910	30.9156						−2.04491	
$(2p16d)^1P_1^o$	16.24485313			−0.24488863	30.9443						−2.05882	
$(2p17d)^1P_1^o$	17.27398677			−0.27402227	30.9681						−2.08818	
$(2p18d)^1P_1^o$	18.30732396			−0.30735946	30.9881						−2.13133	
$(2p19d)^1P_1^o$	19.34503370			−0.34506920	31.0051						−2.17179	
$(2p20d)^1P_1^o$	20.38717585			−0.38721135	31.0196						−2.21833	

polarizations of photoelectrons. Resonance energies E_r and widths Γ_r of all five Rydberg series, $(2pns)^1P_1^o$, $(2pns)^3P_1^o$, $(2pnd)^1P_1^o$, $(2pnd)^3P_1^o$, and $(2pnd)^3D_1^o$, of low-lying doubly excited states of the B^+ ion are studied in detail including electron-correlation and relativistic effects. The angular-distribution and spin-polarization parameters $\{\beta, \xi, \eta, \zeta\}$, which have pronounced variations in the vicinity of each double-excitation resonance, display primarily three classes of characteristic behaviors, namely, A-type for *allowed* resonances $(2pns)^1P_1^o$ and $(2pnd)^1P_1^o$, F-type for *forbidden* resonances $(2pns)^3P_1^o$ and $(2pnd)^3P_1^o$, and M-type for *forbidden* resonances $(2pnd)^3D_1^o$ with large spin-orbit coupling effects.

Table 3: Comparison of resonance widths Γ_r (in $a[-b] = a\times 10^{-b}$ eV) of doubly excited states $(2pns)^1P_1^o$ and $(2pnd)^1P_1^o$ of B^+ from theories and experiments.

State	Present	[9]	[12]	[15]	State	Present	[9]	[12]	[15]
					$(2p3d)^1P_1^o$	5.1662 [−2]	0.0338	0.0312	0.034(2)
$(2p4s)^1P_1^o$	2.6625 [−1]	0.241	0.2453	0.22(1)	$(2p4d)^1P_1^o$	2.2066 [−2]	0.0178	0.0141	0.016(2)
$(2p5s)^1P_1^o$	1.1884 [−1]	0.110	0.1153	0.106(7)	$(2p5d)^1P_1^o$	1.1369 [−2]	0.0101	0.0095	0.010(3)
$(2p6s)^1P_1^o$	6.3431 [−2]	0.059	0.0635	0.048(6)	$(2p6d)^1P_1^o$	6.6047 [−3]	0.0061	0.0064	0.008(3)
$(2p7s)^1P_1^o$	3.7884 [−2]		0.0384	0.029(7)	$(2p7d)^1P_1^o$	4.1691 [−3]		0.0044	0.008(4)
$(2p8s)^1P_1^o$	2.4421 [−2]		0.0249	0.020(6)	$(2p8d)^1P_1^o$	2.7948 [−3]		0.0031	0.001(6)
$(2p9s)^1P_1^o$	1.6628 [−2]		0.0171	0.04(1)	$(2p9d)^1P_1^o$	1.9600 [−3]		0.0023	0.005(8)
$(2p10s)^1P_1^o$	1.1792 [−2]		0.0122	0.02(2)	$(2p10d)^1P_1^o$	1.4224 [−3]		0.0017	
$(2p11s)^1P_1^o$	8.6287 [−3]		0.0090		$(2p11d)^1P_1^o$	1.0597 [−3]		0.0013	
$(2p12s)^1P_1^o$	6.4650 [−3]		0.0069		$(2p12d)^1P_1^o$	8.0546 [−4]		0.0011	
$(2p13s)^1P_1^o$	4.9271 [−3]				$(2p13d)^1P_1^o$	6.2136 [−4]			
$(2p14s)^1P_1^o$	3.8080 [−3]				$(2p14d)^1P_1^o$	4.8446 [−4]			
$(2p15s)^1P_1^o$	2.9780 [−3]				$(2p15d)^1P_1^o$	3.8033 [−4]			
$(2p16s)^1P_1^o$	2.3560 [−3]				$(2p16d)^1P_1^o$	2.9932 [−4]			
$(2p17s)^1P_1^o$	1.8842 [−3]				$(2p17d)^1P_1^o$	2.3491 [−4]			
$(2p18s)^1P_1^o$	1.5206 [−3]				$(2p18d)^1P_1^o$	1.8234 [−4]			
$(2p19s)^1P_1^o$	1.2342 [−3]				$(2p19d)^1P_1^o$	1.3760 [−4]			
$(2p20s)^1P_1^o$	9.9928 [−4]				$(2p20d)^1P_1^o$	9.6857 [−5]			

Table 4: Effective quantum numbers ν, quantum defects μ, resonance energies E_r (in eV), and resonance widths Γ_r (in $a[-b] = a \times 10^{-b}$ eV) of doubly excited states $(2pns)^3P_1^o$ of B^+ from the MCRRPA calculation.

State	ν	μ	E_r(eV)	Γ_r(eV)
$(2p4s)^3P_1^o$	3.49886452	0.50102897	26.7050	3.1666 [−3]
$(2p5s)^3P_1^o$	4.50647877	0.49341472	28.4707	2.2077 [−3]
$(2p6s)^3P_1^o$	5.51095458	0.48893891	29.3586	1.4766 [−3]
$(2p7s)^3P_1^o$	6.51427249	0.48562100	29.8680	1.0529 [−3]
$(2p8s)^3P_1^o$	7.51718124	0.48271226	30.1874	8.2485 [−4]
$(2p9s)^3P_1^o$	8.51997402	0.47991948	30.4008	7.1353 [−4]
$(2p10s)^3P_1^o$	9.52274311	0.47715038	30.5504	6.7072 [−4]
$(2p11s)^3P_1^o$	10.52545978	0.47443371	30.6593	6.6420 [−4]
$(2p12s)^3P_1^o$	11.52799675	0.47189674	30.7410	6.7133 [−4]
$(2p13s)^3P_1^o$	12.53029879	0.46959470	30.8039	6.7618 [−4]
$(2p14s)^3P_1^o$	13.53230180	0.46759169	30.8533	6.7006 [−4]
$(2p15s)^3P_1^o$	14.53396478	0.46592871	30.8929	6.5118 [−4]
$(2p16s)^3P_1^o$	15.53535434	0.46453915	30.9250	6.2169 [−4]
$(2p17s)^3P_1^o$	16.53651255	0.46338095	30.9515	5.8588 [−4]
$(2p18s)^3P_1^o$	17.53755426	0.46233923	30.9736	5.4804 [−4]
$(2p19s)^3P_1^o$	18.53863090	0.46126259	30.9922	5.1127 [−4]
$(2p20s)^3P_1^o$	19.53981972	0.46007377	31.0080	4.7834 [−4]

Table 5: Effective quantum numbers ν, quantum defects μ, resonance energies E_r (in eV), and resonance widths Γ_r (in $a[-b] = a \times 10^{-b}$ eV) of doubly excited states $(2pnd)^3P_1^o$ of B^+ from the MCRRPA calculation.

State	ν	μ	E_r(eV)	Γ_r(eV)
$(2p3d)^3P_1^o$	3.01169305	−0.01174631	25.1505	5.7916 [−2]
$(2p4d)^3P_1^o$	4.00040202	−0.00045527	27.7498	2.6153 [−2]
$(2p5d)^3P_1^o$	4.99656346	0.00338328	28.9706	1.3576 [−2]
$(2p6d)^3P_1^o$	5.99639543	0.00355132	29.6370	7.8561 [−3]
$(2p7d)^3P_1^o$	6.99873582	0.00121093	30.0394	4.9165 [−3]
$(2p8d)^3P_1^o$	8.00324320	−0.00329645	30.3008	3.2572 [−3]
$(2p9d)^3P_1^o$	9.00993439	−0.00998764	30.4801	2.2500 [−3]
$(2p10d)^3P_1^o$	10.01894075	−0.01899400	30.6083	1.6047 [−3]
$(2p11d)^3P_1^o$	11.03048438	−0.03053763	30.7032	1.1743 [−3]
$(2p12d)^3P_1^o$	12.04477723	−0.04483048	30.7754	8.7870 [−4]
$(2p13d)^3P_1^o$	13.06207788	−0.06213113	30.8315	6.7093 [−4]
$(2p14d)^3P_1^o$	14.08255995	−0.08261320	30.8761	5.2178 [−4]
$(2p15d)^3P_1^o$	15.10650188	−0.10655513	30.9120	4.1276 [−4]
$(2p16d)^3P_1^o$	16.13412774	−0.13418099	30.9414	3.3160 [−4]
$(2p17d)^3P_1^o$	17.16567630	−0.16572955	30.9658	2.7007 [−4]
$(2p18d)^3P_1^o$	18.20134937	−0.20140262	30.9862	2.2275 [−4]
$(2p19d)^3P_1^o$	19.24138849	−0.24144174	31.0035	1.8576 [−4]
$(2p20d)^3P_1^o$	20.28601671	−0.28606996	31.0183	1.5654 [−4]

The positions of resonance energies E_r are in general agreement with previous experiments and theoretical calculations. The B^+ ion with a low nuclear charge behaves more or less nonrelativistically, only two of the five resonance series dominate the photoionization cross section. Therefore, experimental data are only available for the energies E_r and widths Γ_r of two singlet Rydberg series $(2pns)^1P_1^o$ and $(2pnd)^1P_1^o$ and do not provide much information on the triplet Rydberg series. Consequently, the MCRRPA results for resonance structures in general agree well with previous nonrelativistic theoretical and experimental results, apart from the extremely sharp resonances for triplet Rydberg series. However, it is possible to experimentally obtain

Table 6: Effective quantum numbers ν, quantum defects μ, resonance energies E_r (in eV), and resonance widths Γ_r (in $a[-b] = a \times 10^{-b}$ eV) of doubly-excited states $(2pnd)^3D_1^o$ of B^+ from the MCRRPA calculation.

State	ν	μ	E_r(eV)	Γ_r(eV)
$(2p4d)^3D_1^o$	3.95032905	0.04961770	27.6630	6.4052 [−4]
$(2p5d)^3D_1^o$	4.95151535	0.04843140	28.9308	2.1109 [−4]
$(2p6d)^3D_1^o$	5.95309632	0.04685043	29.6149	1.1973 [−4]
$(2p7d)^3D_1^o$	6.95516111	0.04478564	30.0255	9.9782 [−5]
$(2p8d)^3D_1^o$	7.95771747	0.04222927	30.2911	1.0149 [−4]
$(2p9d)^3D_1^o$	8.96071925	0.03922750	30.4727	1.1066 [−4]
$(2p10d)^3D_1^o$	9.96407888	0.03586787	30.6023	1.2114 [−4]
$(2p11d)^3D_1^o$	10.96768768	0.03225907	30.6981	1.2967 [−4]
$(2p12d)^3D_1^o$	11.97143623	0.02851052	30.7708	1.3501 [−4]
$(2p13d)^3D_1^o$	12.97522199	0.02472476	30.8272	1.3728 [−4]
$(2p14d)^3D_1^o$	13.97894846	0.02099829	30.8720	1.3730 [−4]
$(2p15d)^3D_1^o$	14.98255856	0.01738819	30.9081	1.3584 [−4]
$(2p16d)^3D_1^o$	15.98600505	0.01394170	30.9375	1.3417 [−4]
$(2p17d)^3D_1^o$	16.98928921	0.01065753	30.9620	1.3295 [−4]
$(2p18d)^3D_1^o$	17.99240347	0.00754328	30.9824	1.3334 [−4]
$(2p19d)^3D_1^o$	18.99541257	0.00453418	30.9997	1.3705 [−4]
$(2p20d)^3D_1^o$	19.99837621	0.00157054	31.0144	1.4764 [−4]

both energies and widths of the triplet Rydberg series $(2pns)^3P_1^o$, $(2pnd)^3P_1^o$, and $(2pnd)^3D_1^o$ by measuring the photoelectron angular-distribution parameter β. Nevertheless, for this purpose, spin-polarization measurements of photoelectrons could always be independent verifications. Experimental studies on angular distribution of photoelectrons are suggested to obtain information on widths of some states, which cannot be obtained from total cross section measurements.

Acknowledgment

This paper was supported in part by the National Science Council of Taiwan under Grant no. NSC99-2112-M-001-023.

References

[1] H.-C. Chi, K.-N. Huang, and K. T. Cheng, "Autoionizing levels of beryllium from the multiconfiguration relativistic random-phase approximation," *Physical Review A*, vol. 43, no. 5, pp. 2542–2545, 1991.

[2] L.-R. Wang, J.-T. Hsiao, and K.-N. Huang, "Doubly excited states of the Be atom in the MCRRPA," *Journal of Physics B*, vol. 39, no. 9, pp. L217–L224, 2006.

[3] J.-T. Hsiao, L.-R. Wang, H.-L. Sun, S.-F. Lin, C.-L. Lu, and K.-N. Huang, "Photoionization processes of the beryllium atom," *Physical Review A*, vol. 78, no. 1, Article ID 013411, 2008.

[4] E. W. B. Dias, H. S. Chakraborty, P. C. Deshmukh, and S. T. Manson, "Relativistic effects in the photoionization of atomic beryllium," *Journal of Physics B*, vol. 32, no. 14, pp. 3383–3389, 1999.

[5] A. A. Wills, T. W. Gorczyca, N. Berrah et al., "Importance of spin-orbit effects in parity-unfavored photoionization of neon, observed using a two-dimensional photoelectron imaging technique," *Physical Review Letters*, vol. 80, no. 23, pp. 5085–5088, 1998.

[6] H.-C. Chi and K.-N. Huang, "Photoionization of beryllium in the multiconfiguration relativistic random-phase approximation," *Physical Review A*, vol. 43, no. 9, pp. 4742–4745, 1991.

[7] M. D. Lindsay, L. T. Cai, G. W. Schinn, C. J. Dai, and T. F. Gallagher, "Angular distribution of ejected electrons from autoionizing 3pns states of magnesium," *Physical Review A*, vol. 45, no. 1, pp. 231–241, 1992.

[8] H.-C. Chi and K.-N. Huang, "Photoionization of magnesium including double excitations," *Physical Review A*, vol. 50, no. 1, pp. 392–398, 1994.

[9] J. A. Tully, M. Le Dourneuf, and C. J. Zeippen, "Photoionisation of the B+('Se) ground state," *Astronomy and Astrophysics*, vol. 211, pp. 485–494, 1989.

[10] J. A. Tully, M. J. Seaton, and K. A. Berrington, "Atomic data for opacity calculations. 14. The beryllium sequence," *Journal of Physics B*, vol. 23, no. 21, p. 3811, 1990.

[11] T. N. Chang and L. Zhu, "Photoionization of the Be isoelectronic sequence from the ground and the ^1s bound excited states," *Physical Review A*, vol. 51, no. 1, pp. 374–380, 1995.

[12] D. S. Kim and S. T. Manson, "Photoionization of the ground-state Be-like B ion leading to the $n = 2$ and $n = 2$ states of B," *Journal of Physics B*, vol. 37, no. 19, pp. 4013–4024, 2004.

[13] J. M. Esteva, *Thése Doctorat d'Etat*, Doctoral thesis, Université Paris XI, AO du CNRS no. 9976, 1974.

[14] E. Jannitti, F. Pinzhong, and G. Tondello, "The absorption spectrum of B II in the vacuum ultraviolet," *Physica Scripta*, vol. 33, no. 5, p. 434, 1986.

[15] S. Schippers, A. Müller, B. M. McLaughlin et al., "Photoionization studies of the B valence shell: experiment and theory," *Journal of Physics B*, vol. 36, no. 16, pp. 3371–3381, 2003.

[16] W. R. Johnson and K.-N. Huang, "Resonance transitions of Be-like ions from multiconfiguration relativistic random-phase approximation," *Physical Review Letters*, vol. 48, no. 5, pp. 315–318, 1982.

[17] K.-N. Huang and W. R. Johnson, "Resonance transitions of mg- and zn-like ions from multiconfiguration relativistic random-phase approximation," *Nuclear Instruments and Methods in Physics Research. Section B*, vol. 9, no. 4, pp. 502–504, 1984.

[18] H.-S. Chou, K.-N. Huang, and W. R. Johnson, "Magnetic dipole transitions of Pb-like ions from the multiconfiguration relativistic random-phase approximation," *Physical Review A*, vol. 44, no. 5, pp. R2769–R2770, 1991.

[19] H.-S. Chou and K.-N. Huang, "Relativistic excitation energies and oscillator strengths for the $6s^2 {}^1s_0 \rightarrow 6s6p {}^1p_1, {}^3p_1$ transitions in Hg-like ions," *Physical Review A*, vol. 45, no. 3, pp. 1403–1406, 1992.

[20] T. C. Cheng and K.-N. Huang, "Resonance transitions of Zn-like ions from the multiconfiguration relativistic random-phase approximation," *Physical Review A*, vol. 45, no. 7, pp. 4367–4373, 1992.

[21] H.-S. Chou and K.-N. Huang, "Relativistic excitation energies and oscillator strengths for the $(5s^2)^1S_0 \rightarrow (5s5p)^1p_1, {}^3P_1$ transitions in Cd-like ions," *Physical Review A*, vol. 46, no. 7, pp. 3725–3729, 1992.

[22] H.-S. Chou, H.-C. Chi, and K.-N. Huang, "Core-polarization effects for the $(6s^2)^1S_0$to$(5s5p)^3p_1^0$, $^1P_1^0$ transitions in Hg-like ions," *Journal of Physics B*, vol. 26, no. 15, pp. 2303–2309, 1993.

[23] H.-S. Chou, H.-C. Chi, and K.-N. Huang, "Relativistic excitation energies and oscillator strengths including core-polarization effects for the intercombination and resonance transitions in Mg-like ions," *Journal of Physics B*, vol. 26, no. 22, pp. 4079–4089, 1993.

[24] H.-S. Chou, H.-C. Chi, and K.-N. Huang, "Core-polarization effects for the intercombination and resonance transitions in Cd-like ions," *Physical Review A*, vol. 48, no. 3, pp. 2453–2456, 1993.

[25] H.-S. Chou, H.-C. Chi, and K.-N. Huang, "Core-polarization effects in the $^3p_1^0 ... ^1P_1^0$ separations of Cd- and Hg-like ions," *Physics Letters A*, vol. 182, no. 2-3, pp. 302–304, 1993.

[26] H.-S. Chou, H.-C. Chi, and K.-N. Huang, "Core polarization effects on the intercombination and resonance transitions in Be-like ions," *Chinese Journal of Physics*, vol. 32, no. 3, pp. 261–268, 1994.

[27] H.-S. Chou, H.-C. Chi, and K.-N. Huang, "Relativistic excitation energies and oscillator strengths for transitions in Zn-like ions including core-polarization effects," *Physical Review A*, vol. 49, no. 4, pp. 2394–2398, 1994.

[28] K.-N. Huang, H.-C. Chi, and H.-S. Chou, "The MCRRPA theory and its applications to photoexcitation and photoionization," *Chinese Journal of Physics*, vol. 33, no. 6, pp. 565–644, 1995.

[29] H.-S. Chou and K.-N. Huang, "Core-shielding effects on photoexcitation of the Hg-like ions," *Chinese Journal of Physics*, vol. 35, no. 1, pp. 35–46, 1997.

[30] C. Y. Hwang, H.-C. Chi, and K.-N. Huang, "Autoionizing levels of zinc from the multiconfiguration relativistic random-phase approximation," *Physical Review A*, vol. 44, no. 11, pp. 7189–7194, 1991.

[31] C. M. Wu, H.-C. Chi, and K.-N. Huang, "Double-excitation effects on the angular distribution of photoelectrons from strontium," *Physical Review A*, vol. 46, no. 3, pp. 1680–1683, 1992.

[32] C.-M. Wu, H.-C. Chi, and K.-N. Huang, "Photoionization of strontium above the $5p_{3/2}$ threshold using the multiconfiguration relativistic random-phase approximation," *Journal of Physics B*, vol. 27, no. 17, p. 3927, 1994.

[33] L.-R. Wang, H.-C. Chi, and K.-N. Huang, "Spin-orbit and core-shielding effects on double-excitation resonances of Zn," *Physical Review Letters*, vol. 83, no. 4, pp. 702–705, 1999.

[34] L.-R. Wang and K.-N. Huang, "Asymmetry and spin polarization parameters of photoelectrons from the Zn atom," *Journal of the Chinese Chemical Society*, vol. 48, pp. 343–345, 2001.

[35] J. T. Hsiao, H. T. Shiao, and K.-N. Huang, "Doubly-excited triplet Rydberg series of the B ion," *Chinese Journal of Physics*, vol. 47, no. 2, pp. 173–183, 2009.

[36] K.-N. Huang and W. R. Johnson, "Multiconfiguration relativistic random-phase approximation. Theory," *Physical Review A*, vol. 25, no. 2, pp. 634–649, 1982.

[37] K.-N. Huang, "Atoms as sources of multipole radiation," *American Journal of Physics*, vol. 62, pp. 73–78, 1994.

[38] K.-N. Huang, "Theory of angular distribution and spin polarization of photoelectrons," *Physical Review A*, vol. 22, pp. 223–239, 1980.

[39] K.-N. Huang, "Kinematic analysis of photoelectrons from polarized targets with J = 12," *Physical Review Letters*, vol. 48, no. 26, pp. 1811–1814, 1982.

[40] K.-N. Huang, "Addendum to "Theory of angular distribution and spin polarization of photoelectrons"," *Physical Review A*, vol. 26, no. 6, pp. 3676–3678, 1982.

[41] J. Dubau and M. J. Seaton, "Quantum defect theory. 13. Radiative transitions," *Journal of Physics B*, vol. 17, no. 3, pp. 381–403, 1984.

[42] U. Fano, "Effects of configuration interaction on intensities and phase shifts," *Physical Review*, vol. 124, no. 6, pp. 1866–1878, 1961.